Research Square

Preprints are preliminary reports that have not undergone peer review.
They should not be considered conclusive, used to inform clinical practice,
or referenced by the media as validated information.

Gleditsia sinensis galactomannan-based composite hydrogel with exceptional water retention

Yuyu E
Beijing Forestry University
Zeyu Chang
Beijing Forestry University
Wen Li
Guangxi Minzu University
Pengfei Li
Guangxi Minzu University
Fuhou Lei
Guangxi Minzu University
Jianxin Jiang
Beijing Forestry University
Wengui Duan
Guangxi University
Shengguang Yuan
Chinese Academy of Sciences
Kun Wang (wangkun@bjfu.edu.cn)
Beijing Forestry University
Xiaopeng Peng
Chinese Academy of Forestry

Research Article

Keywords: Galactomannan, Hyaluronic acid, Chemical cross-linking, Water retention, Composite hydrogel

Posted Date: November 7th, 2023

DOI: https://doi.org/10.21203/rs.3.rs-3499748/v1

License: This work is licensed under a Creative Commons Attribution 4.0 International License.
Read Full License

Additional Declarations: No competing interests reported.

Abstract

A novel epoxy-cross-linked hyaluronic acid/galactomannan composite hydrogel was prepared from Gleditsia sinensis using various alkyl glycidyl ethers as cross-linking agents. The morphological, physicochemical, and mechanical properties of the obtained hydrogels were comparatively investigated and discussed. The optimal composite hydrogel (GM/HDE/HA) exhibited high storage modulus (210 Pa), loss modulus (27.8 Pa), and water retention properties (95%). Hydrogels with high molecular weight (Mw) hyaluronic acid showed higher water retention properties than those with low-Mw hyaluronic acid (80% water retention properties). The molecular docking simulations of hyaluronic acid confirmed the higher formation energies of the high-Mw hyaluronic acid (-14.98 Kcal/mol) than that of the low-Mw hyaluronic acid (-6.90 Kcal/mol). This study offers a new design strategy for a water retention hydrogel by optimizing the cross-linked dimension with various-length polymer chains as cross-linkers. These remarkable advantages make hydrogels have enormous potential in the application of cosmetics and biomedical.

1. Introduction

Hydrogels are three-dimensional network materials formed by physically and/or chemically crosslinking hydrophilic polymers, capable of immobilizing a large amount of water or biological fluids to provide a moist environment [1–6]. Hydrogels are widely implemented in wound dressing [7], tissue engineering [8], soft electronics [9], and health monitoring [10, 11] due to their desired soft, flexible, and biocompatible [12], becoming a potential candidate material in the biomedical and cosmetic fields. However, the poor water retention of hydrogels is the main obstacle in actual use, with the lack of maintaining a moist condition for sufficient time. Since most polysaccharide-based hydrogels exposed to dry environments inevitably and quickly lose water due to water evaporation, the lost flexibility and functions severely limit their practical applications. Therefore, it is urgent to enhance the water retention capacity of a hydrogel to avoid water evaporation and promote its application in different fields, such as soft electronics, cosmetics, biomedical, and so on. Recently, some researchers introduced glycerol or inorganic salts into the hydrogels to reduce the vapor pressure and improve the water retention property. However, the low biocompatibility hindered their biomedical applications. Polysaccharides are the preferred biobased resources for the preparation of industrial or medical materials mainly due to their high molecular weight, low cost, nontoxicity, biodegradability, and biocompatibility [13, 14]. As one of the natural polysaccharides galactomannan of *Gleditsia sinensis* (GM) is naturally biocompatible and biodegradable non-ionic polysaccharides composed of the linear backbone of 1→4-linked β-D-mannopyranosyl units (M) substituted at O-6 with side chains of 1→6-linked α-D-galactopyranosyl units (G) [2–4]. GM could hydrate and form a colloidal solution of high viscosity characteristics with water, even at extremely low concentrations. The role of GM in water compounds is directly attributable to their hydrophilicity, which in turn is due to their molecular structure. The galactose side chains linked to the mannose backbone interact with surrounding water molecules, resulting in entanglement of the chains between different molecules, increasing viscosity and causing gelation or thickening [15]. Due to its biocompatible,

biodegradable and non-toxic properties, GM is widely used as a versatile polysaccharide in oil-well drilling, textile, cosmetic, food, and pharmaceutical industries [16–18]. GM hydrogels are synthesized through physical or covalent cross-linking biopolymer chains and used as water-retaining agents [19, 20]. The chemical process is versatile to obtain controllable structures and desirable mechanical properties of hydrogels. The cross-linking points in hydrogels might stabilize their network by adjusting the molecular chains of GM closer. Several different agents were proposed, including epichlorohydrin [21], glutaraldehyde [22], borate [23], silane crosslinker [24], and N, N-methylene bisacrylamide [25]. However, the limitation of the high toxicity and residuals of these agents in hydrogel implies that suitable methods do not exist to promote the application of GM hydrogel. Therefore, it is crucial to develop a safe cross-linking agent for the preparation of biocompatible GM hydrogels, in which the length of the cross-linker chemicals is one of the vital factors that influence their properties. The degree of effective cross-linking and hydrophilicity of cross-linkers strongly affect the expandability of hydrogel network structures and mechanical strength. Therefore, it is vitally important to investigate the contribution of cross-linker length to hydrogel properties. 1,4-butane diol diglycidyl ether (BDE) is a diepoxide-based linker [26], widely used in the crosslinking of polysaccharides via epoxide groups present at the two ends of the molecule [27]. Therefore, other types of cross-linker with different chain lengths, such as ethylene glycol diglycidyl ether (EDE) and 1,6-hexane diol diglycidyl ether (HDE), are promising candidates for hydrogel fabrication to explore the influence of the cross-linker structure for the mechanical strength of hydrogel.

Hyaluronan (HA) is an anionic glycosaminoglycan polymer consisting of alternate disaccharide units D-glucuronic acid (GlcA) and N-acetyl-D-glucosamine (GlcNAc) linked by β-1,3- and β-1,4-glycosidic bonds, which existed mainly in the intercellular matrix of most connective tissues, such as synovial fluid, skin and vitreous human, and its excellent biocompatibility [28], degradability [29] and the property of moisture retention that makes it desirable application in the pharmaceutical, medical and cosmetic industries. There are abundant hydroxyl and carboxyl groups on its main chain, which could be effectively connected in a biopolymer mixture to form hydrogels with stable structures [30]. There are some methods for modifying HA via chemical cross-linking, such as amidation, etherification and esterification. Interestingly, HA hydrogels prepared by chemical cross-linking using BDE as cross-linker existed with biocompatibility and non-toxic [31]. The formation of a hydrogel network was constructed via the nucleophilic attack of the H atom of the hydroxyl group of the HA on the electrophilic carbon atom of the epoxy group, which occurred in an aqueous solution under alkaline conditions at both ends or only one. Composite polymers synthesized through BDE cross-linked HA presented different properties, even starting from the same material. The variations in structural parameters could affect variations of physical properties of the hydrogels, such as the molecular weight of the HA, the degree of cross-linking, and the substitution position of the BDE cross-linker on HA. Therefore, the effect of HA molecular weight on the water retention properties of the hydrogels obtained is also crucial. Especially, HA is promising building block of human skin tissues due to its innate water retention capacity in the skin [32]. Although HA-containing hydrogels have been widely reported as functional moisturized materials, their mechanism at the atomic level is still unclear. Aquaporin-3 (AQP_3) is a membrane protein in human skin that responds to the transportation of water and glycerol. Water molecules are difficult to transport through

membranes independently without the assistance of AQP_3. It is significant to analyze the interactions of HA and skin components and understand their synergetic mechanism of maintaining the water of the skin.

Here, the contribution of cross-linker length and HA molecular weight in Gleditsia sinensis GM hydrogels was studied to investigate their tensile and water retention properties by using three types of cross-linker, including ethylene glycol EDE, BDE, and HDE. Density functional theory calculation was preliminary performed to investigate the interactions of HA with different molecular weights and other skin components at the atomic level. This work was expected to provide a reference for preparing a hydrogel with desirable water retention capacity.

2. Experimental section

2.1. Materials

Galactomannan (1800 kDa) was supplied by Shexian Forestry Bureau in Hebei, China, and the purification process was carried out according to the previous literature [22]. Hyaluronic acids (cosmetic grade, high molecular weight, 1400 kDa) were purchased from Dongying First Biochem Industrial Co., Ltd. EDE, BDE and HDE were supplied from Shanghai Macklin Biochemical Co., Ltd. (Shanghai, China). All other analytical grade chemicals were obtained from Shanghai Macklin Biochemical Co., Ltd. (Shanghai, China) and used as purchased without further purification.

2.2. Synthesis of Hydrogels

The hydrogels were prepared via the facile one-step strategy. The free hydroxyl groups present at the positions C2, C3, or C6 of the monosaccharide units could be reacted with an etherifying reagent in the presence of sodium hydroxide as catalyst. Firstly, 1.0 g GM and 1.0 g HA power were mixed and mechanically stirred in 50 mL distilled water at 40 ℃ for 2 h, and then 1.25 g NaOH (40 wt%) was added and constant stirred was continued for 30 min to active the free hydroxyl groups. Subsequently, the GM/HA solution and 2.5 g BDE were added to the above solution and magnetically stirred at 25 ℃ for 10 min until obtaining a uniform mixture. After removing the magnetic stir bar, the glass tube was sealed and placed at 40 ℃ for another 6 h. Finally, the formed hydrogel was carefully washed thoroughly with deionized water to remove the residual NaOH and EDE, and packaged in a sealed bag and stored in desiccator with constant temperature and humidity. For comparison, the other two crosslinkers with different alkyl chain lengths, BDE and HDE, were also used to prepare hydrogel with the same method. Additionally, the effect of the GM dosage on the physicochemical property of hydrogel was also investigated by adding 1, 2, and 3 wt%, respectively, named GM/BDE/HA-1, GM/BDE/HA-2, and GM/BDE/HA-3. In most cases, GM/BDE/HA represents GM/BDE/HA-3 in characterization process without additional statements. The scheme for preparing hydrogel is enumerated (Table S1, Supporting Information).

2.3. Characterization

The freeze-dried hydrogels were ground into a powder before performing Fourier transform infrared spectroscopy (FTIR, Nicolet iS5, Thermo Fisher Scientific, America), which acquired in the 400–4000 cm^{-1} range with potassium bromide (KBr) tablet method. The morphology of the hydrogels was examined using field-emission scanning electron microscope (SEM; SU8010, Hitachi, Japan). The element and chemical structure of hydrogels were measured using X-ray photoelectron spectroscopy (XPS, Thermo Fisher Scientific, America).

2.4. Rheological property test

The rheological analysis was measured using an MCR302 rheometer (Anton Paar Shanghai Trading Co., Ltd) with cone plate (2º, 50 mm diameter). The strain sweep test over different strain (0.01–100%) was carried out with fixed oscillation frequency of 1 Hz to analyze the changes in modulus. A Frequency sweeps (0.1–100 Hz) were performed at 1% strain to investigate the storage modulus (G') and loss modulus (G") .

2.5. Water retention of the hydrogel

The water retention capacity of the hydrogels was evaluated via monitoring of weight changes in environments with different temperatures and humidity. The water retention capacity was calculated using the equation below:

$$Waterretention = \frac{m_t}{m_0} \times 100\%$$

where m_t is the mass of the hydrogel at different moments and m_0 is the initial mass of the hydrogel.

2.6. Molecular docking simulation

The data produced during the molecular docking procedure was investigated using the Molecular Operating Environment (MOE2014) software. the HA molecular structures were developed by ChemDraw software. The target crystal structures for AQP3 were retrieved and created using the Protein Data Bank ((https://www.rcsb.org). The docking of molecules between structural model of the molecules and protein was performed by using MOE dock module.

2.7. Statistical Analysis

All experiments were obtained in triplicate and the data are presented as mean ± standard deviation. Statistical analyzes were conducted using Origin software (Version 2018, OriginLab Inc., USA). One-way analysis of variance (ANOVA) was performed using Tukey's honestly significant difference post hoc test to detect significant differences among means. Values of *$p < 0.05$, **$p < 0.01$, and ***$p < 0.001$ was considered statistically significant.

3. Results and discussion

3.1. Assessment of physical-chemical properties

A facile process was used to prepare a hydrogel with moisturizing properties. The solution was formed by directly mixing GM, BDE, and HA, gradually switching to an elastic solid due to the formation of extensive hydrogen and covalent bonds (Figure S1, Supporting Information). The broad characteristic peaks from 3100 to 3600 cm^{-1} appeared in the hydrogel, indicating the symmetrical stretching vibration of the available hydroxyl groups. The above peaks were obviously weakened since the extensive formation of hydrogen bonding in the hydrogel system [33]. The peak at approximately 2931 cm^{-1} corresponds to the O–H and C–H stretching vibrations (Fig. 1a) [34]. Two distinct peaks at 1140 and 1027 cm^{-1} belonged to C–C–O and C–O–C stretching vibrations of the main chain in the biopolymer [35, 36], respectively, and the absorption bands of GM at 1643 cm^{-1} assigned to H–OH bending [37]. The FTIR spectra of all samples show no significant differences in native GM and HA, indicating that no major functional group transformations occurred during the cross-linking process other than the formation of C–O–C linkages involving hydroxyl groups. However, the thermal stability and mechanical property of hydrogel depend on the size of the biomacromolecule in polymer. The thermal stability of hydrogel was investigated by thermal gravimetric analysis, which was expected to improve after the cross-linking reactions. A long plateau with slight weight loss was observed in the range of 35–200 ℃ due to the elimination of bound water [38]. The decomposition temperature for the hydrogel was exceeded by 230 ℃. The hydrogel was totally oxidized and carbonized between 280 ℃ and 500 ℃ (Fig. 1b). The initial degradation temperature and the peak height corresponding to the maximum weight loss rate by the cross-linker with long chains (HDE) were higher than that of the short one (EDE) (Fig. 1c) [39]. Although almost hydrogel existed the same thermal degradation behaviors at the 220–400 ℃ temperature, the solid residue of the hydrogel with HDE at the end of pyrolysis was obviously increased, indicating that the long chains cross-linker increased the thermal stability of the hydrogel (Fig. 1b). Since the formation of the entangled network was determined by the number of functional groups through inter-and intra-molecule hydrogen and covalent bonds with the etherification agent [40], this result was consistent with the rheological results and directly reflected the same structural changes. Previous studies indicated that the peak positions of C 1s depend on the valence state of the C atom in functional groups, which are extensively used to qualitatively confirm the stage of C [41]. Using the C1s peak as the reference to correct the binding energy of other element peaks. The N 1s (400 eV) peak appeared in the all-composite hydrogel survey, which confirmed that HA was successfully introduced into the hydrogel network (Fig. 1d). Four peaks appeared in the orbit spectrum C 1s of GM/HDE/HA hydrogel, in which three peaks with bending energy of 283.45, 284.9 and eV 286.43, representing C–C C–OH and C–O, respectively, while the appearance of the peak at 287.8 eV is assigned to C = O from carboxyl groups of HA (Fig. 1e). The O 1s signal exists three binding energies of approximately 530.3 531.16 and 533.2 eV (Fig. 1f), corresponding to C–O, C–O–C and C = O, respectively [42, 43]. The peaks C 1s (around 286 eV) and O 1s (around 532.08 eV) of the GM/EDE/HA and GM/BDE/HA hydrogels also have similar results to GM/HDE/HA hydrogel (Figure S2, Supporting information). In terms of the C 1s peak, four characteristic peaks at 283.26, 284.73, 286.17 and 287.88 eV; 283.15, 284.77, 286.4 and 288 eV were found in GM/EDE/HA and GM/BDE/HA hydrogels, respectively, assigned to the C–C, C–OH, C–O and C = O linkages. Meanwhile, three characteristic peaks at 532.48, 531.08, and 530.02 eV; 533.16, 531.46, and 531.46 eV were noted in the O 1s spectra of GM/EDE/HA and GM/BDE/HA hydrogel, respectively, ascribing to the C = O, C–O–C and C–O

connections. Therefore, all of these results further confirmed the successful fabrication of the composite hydrogels.

The construction of morphologies in the hydrogel is tightly bound to the degree of crosslinking reactions, which was visualized from the SEM images after being freezing-dried (Fig. 1g-i). The GM/HDE/HA hydrogel presents an average 200 μm porous structure, which was remarkably increased compared to the GM/EDE/HA and GM/BDE/HA hydrogels. In comparison, the GM/BDE/HA and GM/HDE/HA hydrogels display aggregated layers of various sizes, implying that the mobility of polymer chains increased with the length of alkyl chains in cross-linker since the long distance between two adjacent junctions could benefit the motion of polymer chains and create large spaces in the network, leading to the rich pore structure of the hydrogel. The regular arrangement of layered structures could provide a longer spacer in the network, enhancing the correlations with water molecules. Compared with the structure of the GM/HDE/HA and GM/BDE/HA hydrogel, the GM/EDE/HA hydrogel displayed a thin layered structure and loose pores. It inferred that it is easier for the hydrogel to pile up and form a layered structure with the increasing chain length of the cross-linker. Therefore, crosslinks initiated by the long chains cross-linker were more likely to build a complete layered network structure to impart hydrogel higher mechanical strength.

3.2. Rheological physicochemical properties of hydrogel

The GM contains plenty of hydroxyl groups and plays a crucial role in forming a hydrogel network. In hydrogels, the main interactions binding the polymers are the covalent and hydrogen bonds between hyaluronic acid and galactomannan. Therefore, the cross-linking agent (BDE) was chosen as a cross-linker to prepare a hydrogel to compare the contribution of polysaccharide structures. The results from the frequency sweep experiment at a constant strain of 0.1% indicated that the GM/BDE/HA-1 hydrogel possessed greater storage modulus G' than the loss modulus G" before the angular frequency reached 0.26 rad/s, and conversely, G" was higher than G' as the angular frequency was higher than 0.26 rad/s (Fig. 2a). However, the G's of the GM/BDE/HA-2 and GM/BDE/HA-3 hydrogels at angular frequency surpassed the G"s, indicating the formation of a more stable network and exhibiting a solid-like behavior over the applied frequency range (Fig. 2b and c). The elastic property of the hydrogels was evaluated by stain amplitudes ranging from 0.01–100% at 1 Hz. With increasing strain, all hydrogels possessed higher G' than G" during the whole strain amplitude, presenting the solid-like behavior. Furthermore, the modulus value of GM/BDE/HA-3 hydrogel is obviously higher than the other two hydrogels, indicating that GM could enhance the stability of the network (Fig. 2d, e, and f). The mechanical property of the hydrogel depends on size of the biomacromolecule consisting of an entangled network through covalent and hydrogen bonds [40]. Introducing GM biomacromolecule with abundant hydroxyl groups into the hydrogel network promoted the formation of hydrogen bonds with the HA chain and covalent bonds with the etherifying reagent.

The length of agent cross-linker strongly affects the properties of the hydrogel because the expandability of network structures is a key factors affecting mechanical stress owing to the degree of effective cross-linking and hydrophilicity of the cross-linkers [44]. Therefore, there is an urgent need to investigate the

contribution of cross-linker length to hydrogel properties. Therefore, hydrogels from two kinds of macromolecular cross-linkers (HDE and EDE) with different chain lengths were prepared via the same polymerization process. The comparative rheological curves of the hydrogels with different cross-linkers showed that the hydrogel with EDE is weak (Figs. 3a and c) and that with HDE exhibits excellent mechanical properties (Figs. 3b and d). With respect to the maximum G' and G" values, there was a clear tendency that the hydrogel from the cross-linker with a longer alkyl chain shows higher values. It is probably the fact that abundant functional groups exposed by longer chains in cross-linking agents could insert into the adjacent chains in GM during the dissolving process. This process competitively generated new intramolecular hydrogen bonds with GM and then increased the mechanical properties. Meanwhile, the long alkyl chains provide covalent bond force in the cross-linked network, further enhancing the rigidity and strength of hydrogels. Therefore, the above results revealed that cross-linker length plays a vital role in the mechanical properties of the obtained hydrogel.

3.3. Water retention analysis of the hydrogel

Hydrogels easily lose moisture in the air, which makes them unusable in complex environments [45]. In this paper, the interactions between the cross-linker and HA were utilized to improve the stability of the prepared hydrogel under complicated environmental conditions. The water retention property of the hydrogel is highly dependent on humidity and temperature [46], which was comparatively investigated in this study. Under a drying condition of 25 ℃ and 25% relative humidity (RH), the GM/EDE/HA and GM/BDE/HA hydrogel severely lost water by about 40% and 30% within 14 d, respectively, while GM/HDE/HA hydrogel retained the water content as high as 80% (Figure. 4a). In comparison, the water retention of the GM/EDE/HA hydrogel was 70% within 21 d at 25 ℃ and 50% RH, exceeding 90% and 95% for the GM/BDE/HA and GM/HDE/HA hydrogel, respectively (Figure. 4b). The hydrogel existed a hygroscopic performance in a high-humidity environment owing to the synergistic effect of the GM hydrophilic property and the HA water-retention characteristics. Moreover, GM/HDE/HA hydrogel has the ability to maintain a water content of more than 90% with 21 d under the condition of simulated human skin (36 ℃ and 50% RH) (Figure. 4c). The water retention test resulted in the hydrogel still being able to maintain over 90% of the water content after 21 d in the natural environment, gradually increasing with increasing humidity and length of cross-linker. This implies that longer functional cross-linkers lead to a larger space of the cross-linked network, corresponding to a higher water retention behavior. The results further confirmed that the longer spacer in the cross-linked network could provide more interaction sites for hydrogen bonds between functional groups with water molecules, prolonging water molecules' residence time in the hydrogel network structure to achieve higher water retention. HA could bond water 1000 times its mass via hydrogen bonding to prolong water retention due to its hygroscopic and viscoelastic properties[47]. The effects on water retention of incorporation of a hydrophilic polymer were explored by altering HA molecular weight. At 25 ℃ and 25% RH, the GM/HDE/HA (LMW-HA represent composed of HA with low molecular weight, 1200 kDa) severely lost water by about 30% within 14 d (Figure. 5a), while the GM/HDE/HA hydrogel has ability to maintain a high value of 80% water content within 14 d (Figure. 4a). The water retention rate of GM/HDE/LMW-HA (LMW-HA represent composed of HA with low molecular weight, 1200 kDa) hydrogel exceeded 90% in the high humidity environment of

both 25 ℃ and 50% RH and 36 ℃ and 50% RH (Figure. 5b and c), which are similar to those of the GM/HDE/HA hydrogel. The result indicated that HA with a higher molecular weight could reduce the loss of water molecules in the hydrogel.

3.4. Molecular docking simulations

Structural insights based on molecular docking revealed important subsites that are essentially required to interact with HA to control water transportation. Therefore, to further understand the mechanism of effects of HA with different molecular weights on water retention, the coordination interactions between HA and protein was preliminary investigated by density functional theory calculation. The HA polymers of different molecular weights were created using the ChemDraw software, in which the HA macromolecule consisted of 6, 5, 4, 3, 2, and 1 disaccharide (GlcA-β-1,3-GlcNAc-β-1,4-) units were labeled as HA_6, HA_5, HA_4, HA_3, HA_2, and HA_1, respectively. The optimized geometries from molecular docking (Fig. 6) showed that the formation energies of higher molecular weight HA coordination configuration with the protein are much higher than lower molecular weight HA, corresponding to stronger intra- and inter-molecular H-bond interactions and more stable structure. Specifically, the formation energies between HA and protein decreased from − 6.90 to -14.98 Kcal/mol with increasing HA molecular weight (Supporting information Table S2). Molecular docking results that higher molecular weight HA could adsorb much more residues of AQP_3, and the adsorption behavior of HA on the AQP_3 surface could depend on the hydrophilic residues (Figure. 6f). These interactions between HA molecules and residues of AQP_3 could significantly influence the original gating function of AQP_3 [48]. Additionally, the number of H-bonds formed between the HA polymers was further estimated to investigate the mechanism of the inhibition effect of water permeation rate through AQP_3 from HA. The best-fitting poses adopted by HA molecules are displayed (Fig. 7), and the data on hydrogen bonding between the HA molecules are listed (Supporting Materials, Table S3). In the docking process, the ligand set must have less than 100 heavy atoms; therefore, we only simulated the docking process of four molecular weights of HA, which do not influence the explanation of the mechanism of the interaction force between HA molecules. Molecular Operating Environment (MOE), as the primary mechanism of molecular docking, was carried out to recognize a precise docking study between the target molecule and the compounds. The HA molecules revealed a best-fitting pose through hydrogen bonding with another monosaccharide. The interaction distance ranged from 3.06 to 2.87 Å and the energy stabilization from − 0.9 to -1.9 Kcal/mol. The result indicates that HA with a higher molecular weight could form more intra- and inter-molecular H-bonds than the one with a lower molecular weight. This result could be explained as the monosaccharide in the longer HA has more sites for forming more H-bonds with the adjacent units. Therefore, the reason that HA decreases the mobility of water through the skin is not only the strong interaction between HA and water slowing water permeation, but also could be the potential interaction between HA and the residue of AQP_3, which significantly affecting the exit or entry of water molecules across the skin.

4. Conclusions

The hydrogels were prepared by cross-linking the high- and low-Mw HAs with different length cross-linker (EDE, BDE, and HDE) under alkaline conditions, respectively. The tensile strength and water retention properties of the hydrogels were highly dependent on the concentration of GM, the structure of the cross-linker, and HA's Mw. The hydrogels with a long-length cross-linker and high Mw HA exhibited a higher mechanical strength and water retention (95%). The molecular docking simulation with MOE2014 software was used to investigate the effect of the HA Mw on water retention. The results showed that HA polymers could affect water molecules across the skin, which presents potential biomaterials in the biomedical and cosmetic fields.

Declarations

CRediT authorship contribution statement

Conceptualization, YY. E., XP. P., and K.W.; methodology, YY. E. and K.W.; formal analysis, YY. E., ZY. C. and K.W.; investigation, W. L., SG. Y., and K.W.; resources, K.W. and JX. J.; writing – original draft preparation, YY. E., and K.W.; writing – review and editing, W. L., PE. L., FH. L., and XP. P.; supervision, K.W., JX. J. and W. L.; project administration, K.W.; funding acquisition, K.W.

Declaration of competing interest

The authors declare that they have no known competing financial interests or personal relationships that could have appeared to influence the work reported in this paper.

Funding

This work was financially supported by the National Key Research and Development Program of China (2022YFD2200804), and the Guangxi Key Laboratory of Chemistry Engineering of Forest Products (GXFK2306).

Data availability

The data and materials in this study are all available from the corresponding authors upon request.

References

1. Cruz-Acuña R, García AJ (2017) Synthetic hydrogels mimicking basement membrane matrices to promote cell-matrix interactions. Matrix Biol 57 – 58:324 – 333. https://doi.org/10.1016/j.matbio.2016.06.002
2. Madl CM, Heilshorn SC (2018) bioorthogonal strategies for engineering extracellular matrices. Adv Funct Mater 28:1706046. https://doi.org/10.1002/adfm.201706046
3. Mo C, Xiang L, Chen Y (2021) Advances in injectable and self-healing polysaccharide hydrogel based on the schiff base reaction. Macromol Rapid Comm 42:2100025.

https://doi.org/10.1002/marc.202100025

4. Nurkesh A, Jaguparov A, Jimi S, Saparov A (2020) Recent advances in the controlled release of growth factors and cytokines for improving cutaneous wound healing. Front Cell Dev Biol 8:638. https://doi.org/10.3389/fcell.2020.00638
5. Wang H, Heilshorn SC Adaptable hydrogel networks with reversible linkages for tissue engineering. Adv Mater 27:3717–3736. https://doi.org/10.1002/adma.201501558
6. Zhao F, Bae J, Zhou X, Guo Y, Yu G (2018) Nanostructured functional hydrogels as an emerging platform for advanced energy technologies. Adv Mater 30:1801796. https://doi.org/10.1002/adma.201801796
7. Sudheesh Kumar PT, Lakshmanan VK, Anilkumar TV, Ramya C, Reshmi P, Unnikrishnan AG, Nair SV, Jayakumar R (2012) Flexible and microporous chitosan hydrogel/nano ZnO composite bandages for wound dressing: in vitro and in vivo evaluation. ACS Appl Mater Interfaces 4:2618–2629. https://doi.org/10.1021/am300292v
8. Nasri-Nasrabadi B, Kaynak A, Heidarian P, Komeily-Nia Z, Mehrasa M, Salehi H, Kouzani AZ (2018) Sodium alginate/magnesium oxide nanocomposite scaffolds for bone tissue engineering. Polym Adv Technol 29:2553–2559. https://doi.org/10.1002/pat.4367
9. Lin N, Gèze A, Wouessidjewe D, Huang J, Dufresne A (2016) Dufresne, Biocompatible double-membrane hydrogels from cationic cellulose nanocrystals and anionic alginate as complexing drugs codelivery. ACS Appl Mater Interfaces 8:6880–6889. https://doi.org/10.1021/acsami.6b00555
10. Boutry CM, Beker L, Kaizawa Y, Vassos C, Tran H, Hinckley AC, Pfattner R, Niu S, Li J, Claverie J, Wang Z, Chang J, Fox PM, Bao Z (2019) Biodegradable and flexible arterial-pulse sensor for the wireless monitoring of blood flow. Nat Biomed Eng 3:47–57. https://doi.org/10.1038/s41551-018-0336-5
11. Xu S, Jayaraman A, Rogers JA (2019) Skin sensors are the future of health care. Nature. https://doi.org/10.1038/d41586-019-02143-0. 571:319 – 321
12. Liu R, Wang T, Li G, Fan Z, Zhou Q, Wang K, Li P, Huang W (2023) Self-reinforced hydrogel-based skin-contactable flexible electronics for multimodal electrophysiological signal monitoring and emergency alarming system. Adv Funct Mater 33:2214917. https://doi.org/10.1002/adfm.202214917
13. Zhu T, Mao J, Cheng Y, Liu H, Lv L, Ge M, Li S, Huang J, Chen Z, Li H, Yang L, Lai Y (2019) Recent progress of polysaccharide-based hydrogel interfaces for wound healing and tissue engineering. Adv Mater Interfaces 6:1900761. https://doi.org/10.1002/admi.201900761
14. Chen J, Nichols BLB, Norris AM, Frazier CE, Edgar KJ (2020) All-polysaccharide, self-healing injectable hydrogels based on chitosan and oxidized hydroxypropyl polysaccharides. Biomacromolecules 21:4261–4272. https://doi.org/10.1021/acs.biomac.0c01046
15. Li P, Wang T, He J, Jiang J, Lei F (2021) Synthesis, characterization, and selective dye adsorption by pH- and ion-sensitive polyelectrolyte galactomannan-based hydrogels. Carbohyd Polym 264:118009. https://doi.org/10.1016/j.carbpol.2021.118009

16. Paixão MVG, Balaban RDC (2018) Application of guar gum in brine clarification and oily water treatment. Int J Biol Macromol 108. https://doi.org/10.1016/j.ijbiomac.2017.11.166. :119 – 126
17. Gresta F, Trostle C, Sortino O, Santonoceto C, Avola G (2019) Rhizobium inoculation and phosphate fertilization effects on productive and qualitative traits of guar (Cyamopsis tetragonoloba (L.) Taub). Ind Crop Prod 139:111513. https://doi.org/10.1016/j.indcrop.2019.111513
18. González A, Barrera GN, Galimberti PI, Ribotta PD, Alvarez Igarzabal CI (2019) Development of edible films prepared by soy protein and the galactomannan fraction extracted from Gleditsia triacanthos (Fabaceae) seed. Food Hydrocolloid 97:105227. https://doi.org/10.1016/j.foodhyd.2019.105227
19. Chen W, Bu Y, Li D, Liu Y, Chen G, Wan X, Li N (2020) Development of high-strength, tough, and self-healing carboxymethyl guar gum-based hydrogels for human motion detection. J Mater Chem C 8:900–908. https://doi.org/10.1039/c9tc05797h
20. Thombare N, Mishra S, Siddiqui MZ, Jha U, Singh D, Mahajan GR (2018) Design and development of guar gum based novel, superabsorbent and moisture retaining hydrogels for agricultural applications. Carbohyd Polym 185:169–178. https://doi.org/10.1016/j.carbpol.2018.01.018
21. Tang H, Liu Y, Li Y, Li Q, Liu X (2020) Hydroxypropylation of cross-linked sesbania gum, characterization and properties. Int J Biol Macromol 152:1010–1019. https://doi.org/10.1016/j.ijbiomac.2019.10.188
22. Zhao N, Chai Y, Wang T, Wang K, Jiang J, Yang HY (2019) Preparation and physical/chemical modification of galactomannan film for food packaging. Int J Biol Macromol 137:1060–1067. https://doi.org/10.1016/j.ijbiomac.2019.07.048
23. Liu C, Lei F, Li P, Jiang J, Wang K (2020) Borax crosslinked fenugreek galactomannan hydrogel as potential water-retaining agent in agriculture. Carbohyd Polym 236:116100. https://doi.org/10.1016/j.carbpol.2020.116100
24. Butt A, Jabeen S, Nisar N, Islam A, Gull N, Iqbal SS, Khan SM, Yameen B (2019) Controlled release of cephradine by biopolymers based target specific crosslinked hydrogels. Int J Biol Macromol 121:104–112. https://doi.org/10.1016/j.ijbiomac.2018.10.018
25. Ling Z, Gu J, Liu W, Wang K, Huang C, Lai C, Yong Q (2020) Actuating, shape reconstruction, and reinforcement of galactomannan-based hydrogels by coordination bonds induced metal ions capture. Int J Biol Macromol 165:2721–2730. https://doi.org/10.1016/j.ijbiomac.2020.10.059
26. Yang IH, Lin IE, Chen TC, Chen ZY, Kuan CY, Lin JN, Chou YC, Lin FH (2021) Synthesis, characterization, and evaluation of BDDE crosslinked chitosan-TGA hydrogel encapsulated with genistein for vaginal atrophy. Carbohyd Polym 260:117832. https://doi.org/10.1016/j.carbpol.2021.117832
27. Yang B, Guo X, Zang H, Liu J (2015) Determination of modification degree in BDDE-modified hyaluronic acid hydrogel by SEC/MS. https://doi.org/10.1016/j.carbpol.2015.05.050. Carbohyd Polym 131:233 – 239
28. Führmann T, Obermeyer J, Tator CH, Shoichet MS (2015) Click-crosslinked injectable hyaluronic acid hydrogel is safe and biocompatible in the intrathecal space for ultimate use in regenerative

strategies of the injured spinal cord. Methods 84:60–69. https://doi.org/10.1016/j.ymeth.2015.03.023

29. Li L, Wang N, Jin X, Deng R, Nie S, Sun L, Wu Q, Wei Y, Gong C (2014) Biodegradable and injectable in situ cross-linking chitosan-hyaluronic acid based hydrogels for postoperative adhesion prevention. Biomaterials 35:3903–3917. https://doi.org/10.1016/j.biomaterials.2014.01.050
30. Gilarska A, Lewandowska-Łańcucka J, Guzdek-Zając K, Karewicz A, Horak W, Lach R, Wójcik K, Nowakowska M (2020) Bioactive yet antimicrobial structurally stable collagen/chitosan/lysine functionalized hyaluronic acid–based injectable hydrogels for potential bone tissue engineering applications. Int J Biol Macromol 155:938–950. https://doi.org/10.1016/j.ijbiomac.2019.11.052
31. Lan SM, Jou IM, Wu PT, Wu CY, Chen SC (2015) Investigation into the safety of perineural application of 1,4-butanediol diglycidyl ether-crosslinked hyaluronan in a rat model. J Biomed Mater Res B 103:718–726. https://doi.org/10.1002/jbm.b.33251
32. Dong Q, Guo X, Li L, Yu C, Nie L, Tian W, Zhang H, Huang S, Zang H (2020) Understanding hyaluronic acid induced variation of water structure by near-infrared spectroscopy. Sci Rep 10:1387. https://doi.org/10.1038/s41598-020-58417-5
33. Chen J, Li Y, Zhang Y, Zhu Y (2015) Preparation and characterization of graphene oxide reinforced PVA film with boric acid as crosslinker. J Appl Polym Sci 132:42000. https://doi.org/10.1002/app.42000
34. Li P, Wang T, He J, Jiang J, Lei F (2021) Diffusion of water and protein drug in 1,4-butanediol diglycidyl ether crosslinked galactomannan hydrogels and its correlation with the physicochemical properties. Int J Biol Macromol 183:1987–2000. https://doi.org/10.1016/j.ijbiomac.2021.05.195
35. Li D, Yang N, Zhang Y, Guo L, Sang S, Jin Z, Xu X (2018) Structural and physicochemical changes in guar gum by alcohol–acid treatment. Carbohyd Polym 179:2–9. https://doi.org/10.1016/j.carbpol.2017.09.057
36. Mudgil D, Barak S, Khatkar BS (2012) X-ray diffraction, IR spectroscopy and thermal characterization of partially hydrolyzed guar gum. Int J Biol Macromol 50. https://doi.org/10.1016/j.ijbiomac.2012.02.031. :1035 – 1039
37. Chandrika KSVP, Singh A, Rathore A, Kumar A (2016) Novel cross linked guar gum-g-poly(acrylate) porous superabsorbent hydrogels: Characterization and swelling behaviour in different environments. Carbohyd Polym 149:175–185. https://doi.org/10.1016/j.carbpol.2016.04.077
38. Dai Q, Ma J, Ma S, Wang S, Li L, Zhu X, Qiao X (2016) Cationic ionic liquids organic ligands based metal-organic frameworks for fabrication of core–shell microspheres for hydrophilic interaction liquid chromatography. ACS Appl Mater Interfaces 8:21632–21639. https://doi.org/10.1021/acsami.6b04756
39. Uddin KMA, Ago M, Rojas OJ (2017) Hybrid films of chitosan, cellulose nanofibrils and boric acid: flame retardancy, optical and thermo-mechanical properties. Carbohyd Polym 177:13–21. https://doi.org/10.1016/j.carbpol.2017.08.116

40. Browne S, Hossainy S, Healy K (2020) Hyaluronic acid macromer molecular weight dictates the biophysical properties and in vitro cellular response to semisynthetic hydrogels. ACS Biomater Sci Eng 6:1135–1143. https://doi.org/10.1021/acsbiomaterials.9b01419
41. Chang EYY, Lu ZY, Ju JH, Jiang YS, Duan JX, Li WG, Lei PF, Yao FH, Wang X K (2023) Enzymatically mediated Gleditsia sinensis galactomannan based hydrogel inspired by wound healing process. Int J Biol Macromol 230:123152. https://doi.org/10.1016/j.ijbiomac.2023.123152
42. Qin Y, Mo J, Liu Y, Zhang S, Wang J, Fu Q, Wang S, Nie S (2022) Stretchable triboelectric self-Powered sweat sensor fabricated from self-healing nanocellulose hydrogels. Adv Funct Mater 32:2201846. https://doi.org/10.1002/adfm.202201846
43. Jia Z, Zeng Y, Tang P, Gan D, Xing W, Hou Y, Wang K, Xie C, Lu X (2019) Conductive, tough, transparent, and self-healing hydrogels based on catechol-metal ion dual self-catalysis. Chem Mater 31:5625–5632. https://doi.org/10.1021/acs.chemmater.9b01498
44. Sannino A, Maffezzoli A, Nicolais L (2003) Introduction of molecular spacers between the crosslinks of a cellulose-based superabsorbent hydrogel: Effects on the equilibrium sorption properties. J Appl Polym Sci 90:168–174. https://doi.org/10.1002/app.12625
45. Chen F, Zhou D, Wang J, Li T, Zhou X, Gan T, Handschuh-Wang S, Zhou X (2018) Rational fabrication of anti-freezing, non-drying tough organohydrogels by one-pot solvent displacement. Angew Chem Int Ed 57:6568–6571. https://doi.org/10.1002/anie.201803366
46. Sui X, Guo H, Cai C, Li Q, Wen C, Zhang X, Wang X, Yang J, Zhang L (2021) Ionic conductive hydrogels with long-lasting antifreezing, water retention and self-regeneration abilities. Chem Eng J 419:129478. https://doi.org/10.1016/j.cej.2021.129478
47. Hargittai I, Hargittai M (2008) Molecular structure of hyaluronan: an introduction. Struct Chem 19:697–717. https://doi.org/10.1007/s11224-008-9370-3
48. de Almeida A, Martins AP, Mósca AF, Wijma HJ, Prista C, Soveral G, Casini A (2016) Exploring the gating mechanisms of aquaporin-3: new clues for the design of inhibitors? Mol BioSyst 12:1564–1573. ttps://doi.org/10.1039/c6mb00013d

Figures

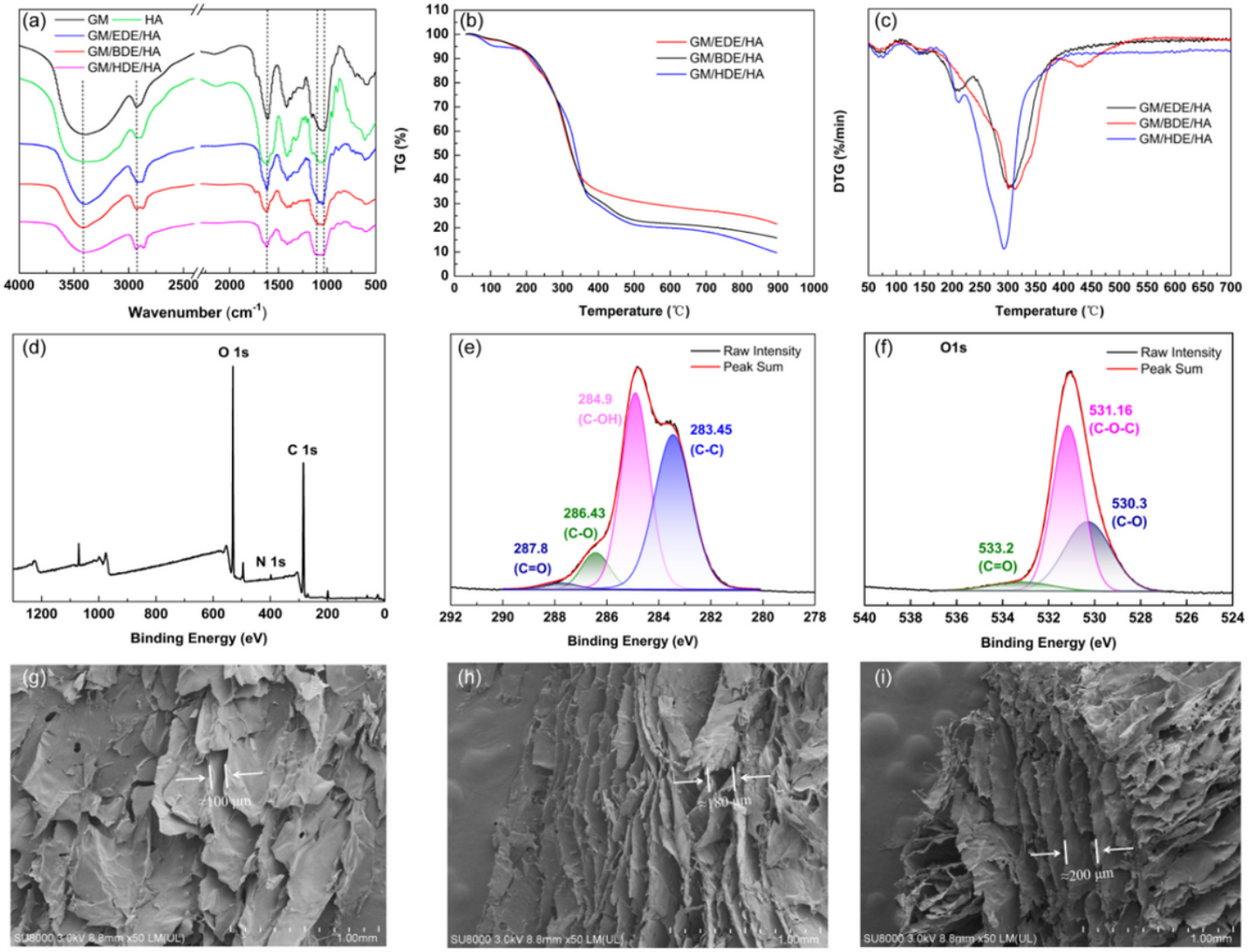


Figure 1

(a) FT-IR, (b) TGA, and (c) DSC of the selected samples; XPS spectra (d) wide scan, (e) C 1s and (f) O 1s of GM/HDE/HA hydrogel; SEM images of (g) GM/EDE/HA, (h) GM/BDE/HA and (i) GM/HDE/HA hydrogels.

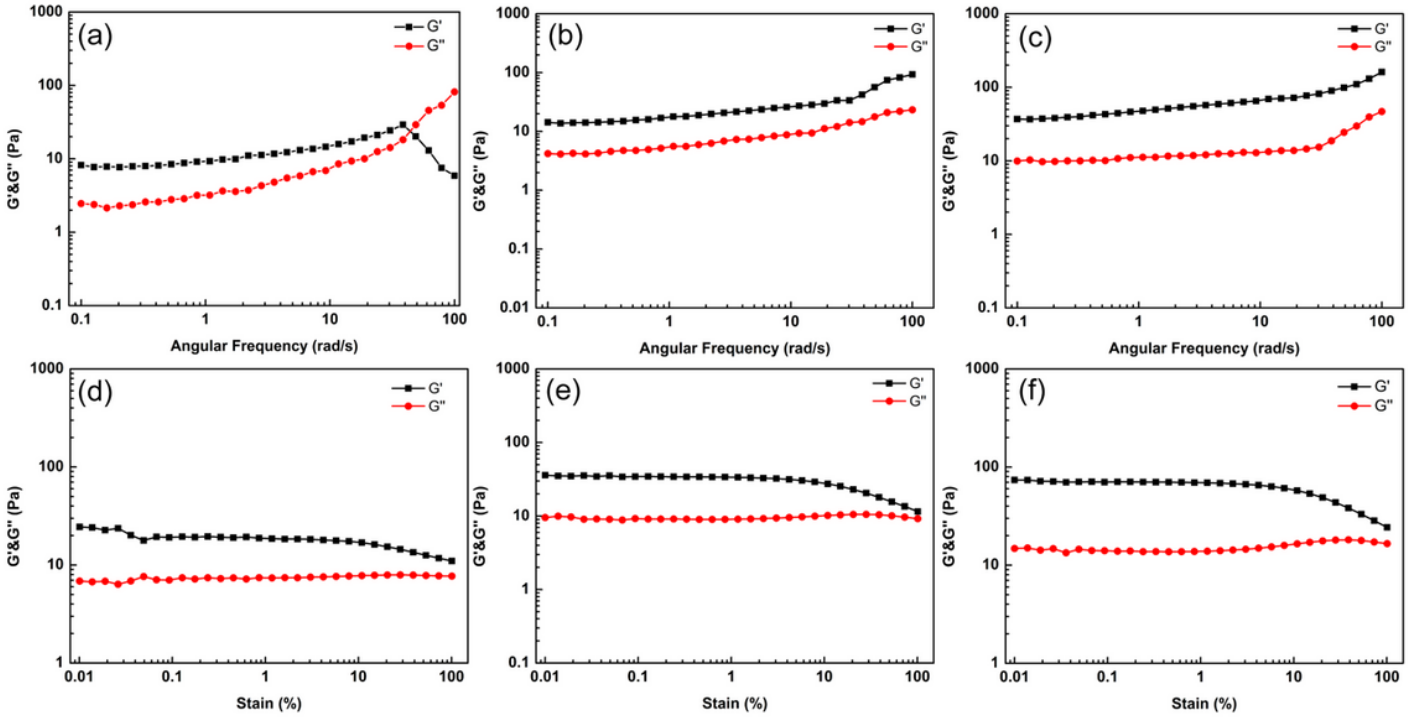


Figure 2

Rheological characteristics of GM/BDE/HA-1 (a and d), GM/BDE/HA-2 (b and e) and GM/BDE/HA-3 (c and f) hydrogels at different angular frequency and shear strain.

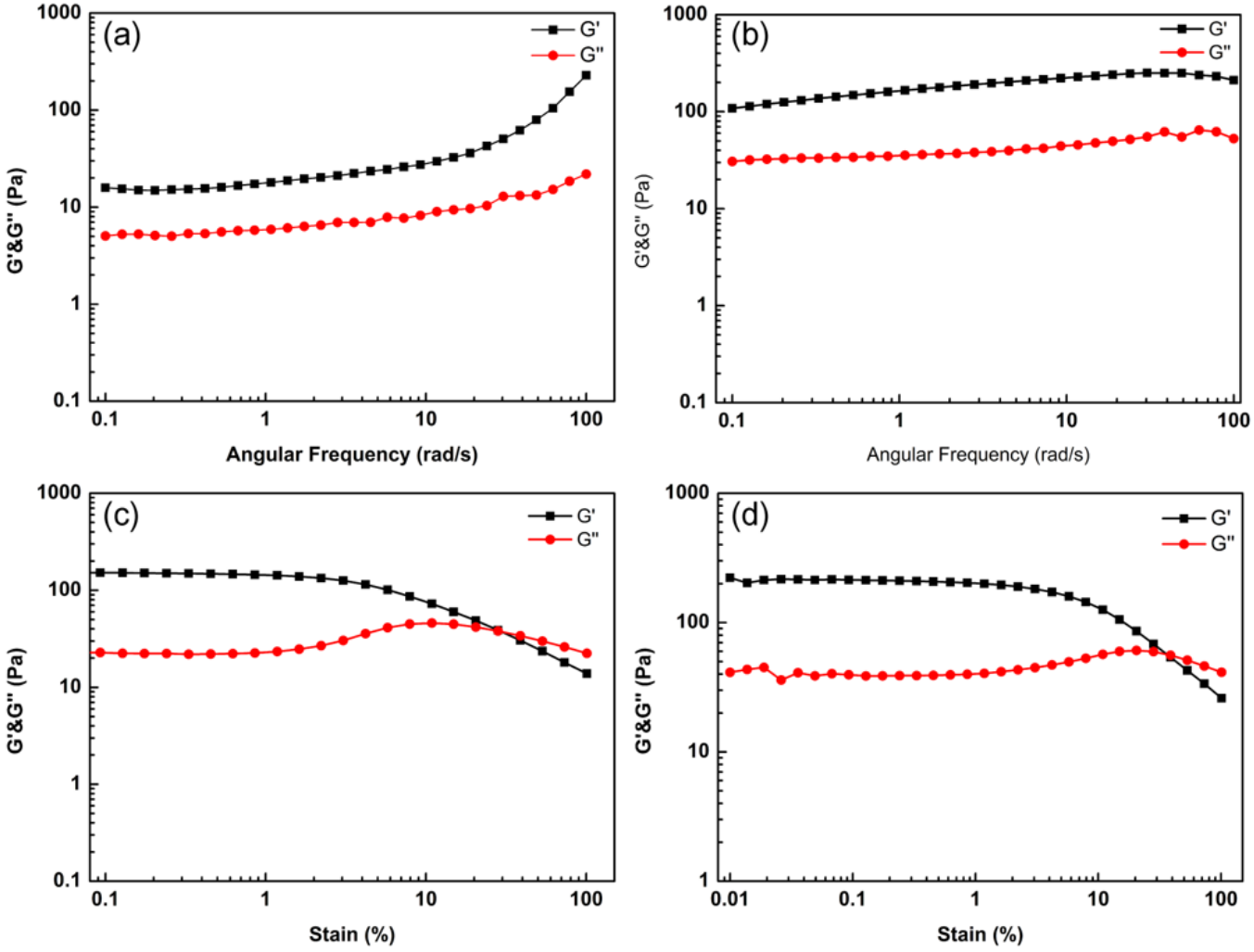


Figure 3

Rheological characteristics of GM/EDE/HA (a and c) and GM/HDE/HA (b and d) hydrogels at different angular frequency and shear strain.

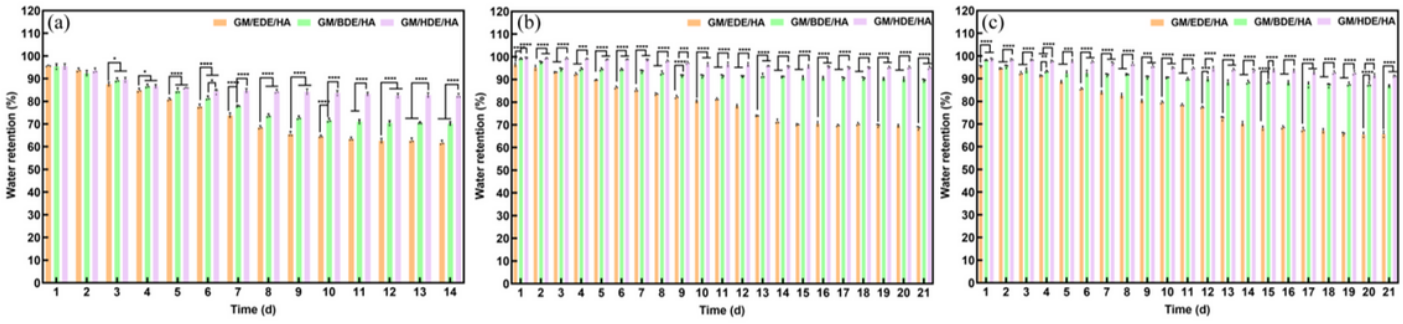


Figure 4

Water retention rate of GM/EDE/HA, GM/BDE/HA and GM/HDE/HA hydrogel stored for (a) 14 d at 25 ℃ and 25% RH; (b) 21 d at 25 ℃ and 50% RH; and (c) 21 d at 36 ℃ and 50% RH.

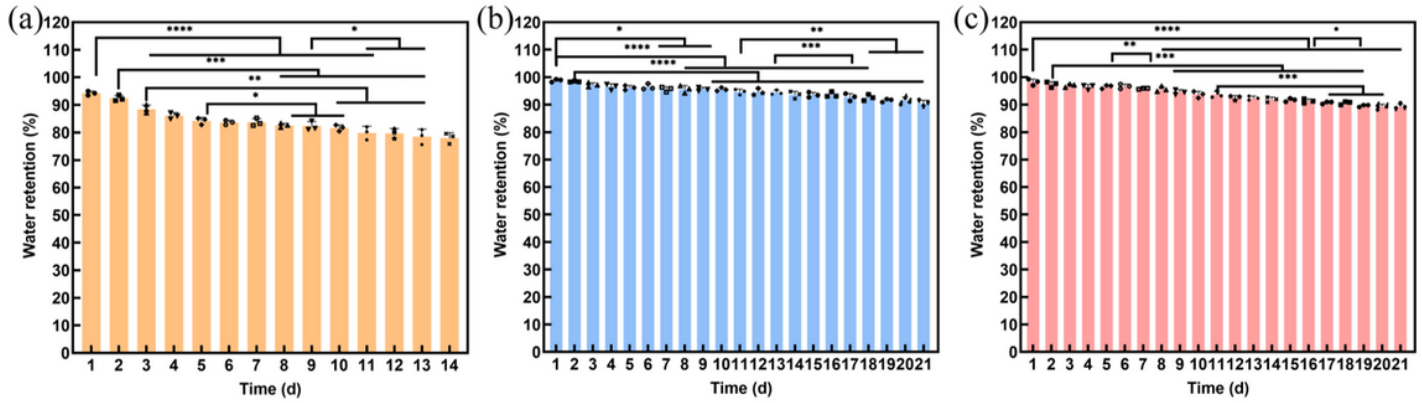


Figure 5

Water retention rate of GM/HDE/LMW-HA stored for (a) 14 d at 25 ℃ and 25% RH; (b) 21 d at 25 ℃ and 50% RH; and (c) 21 d at 36 ℃ and 50% RH.

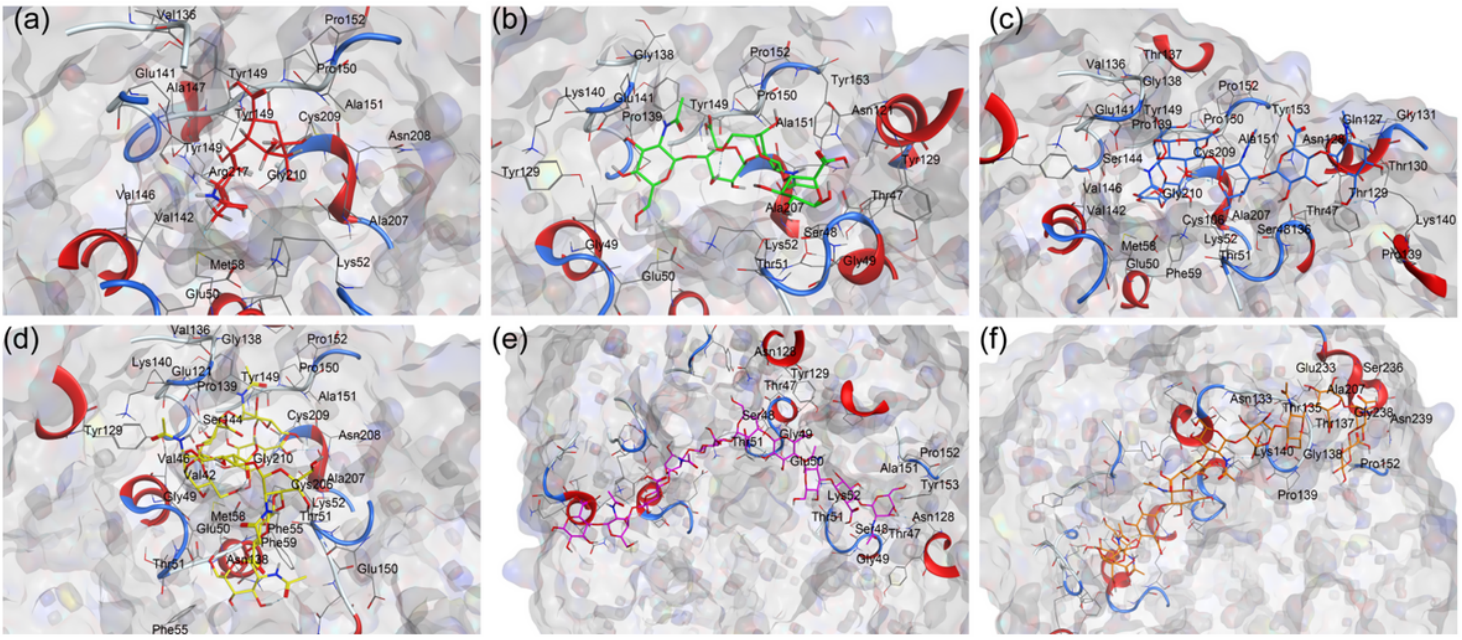


Figure 6

3D molecular docking of the interaction between protein (AQP_3) and (a) HA_1, (b) HA_2, (c) HA_3, (d) HA_4, (e) HA_5 and (f) HA_6, respectively.

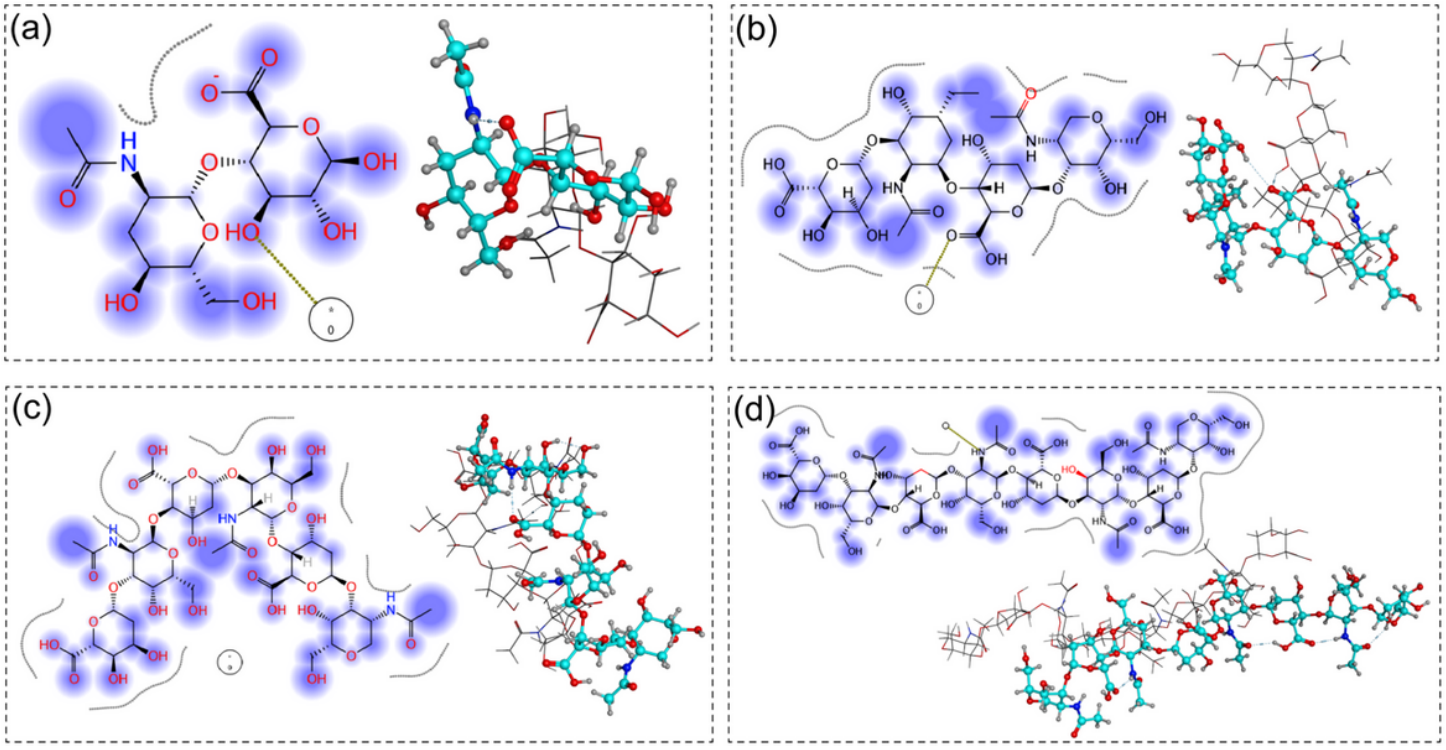


Figure 7

3D docking and 2D diagrams of compound (a) HA_1, (b) HA_2, (c) HA_3 and (d) HA_4.

Supplementary Files

This is a list of supplementary files associated with this preprint. Click to download.

- SupportingInformation.docx